Cofunction of Protons as Dopant and Reactant Activate the Electrocatalytic Hydrogen Evolution in Emeraldine-Polyguanine

Halime Coskun,* Abdalaziz Aljabour, Wolfgang Schöfberger, Andreas Hinterreiter, David Stifter, Niyazi Serdar Sariciftci, and Philipp Stadler

Functional conductive polymers represent an emerging class of nonmetallic electrocatalysts attractive to substitute scarce and expensive elements used today. Here the synthesis of emeraldine-polyguanine as structural-molecular analog to polyaniline is shown and the conducting biopolymer as molecular hydrogen electrocatalyst is applied. The polymerized and protonated nucleobase aids the catalytic electroreduction of protons over a peculiar mechanism, where, over amino-association, protons coserve as dopant and reactant. In acidic media the electrocatalytic evolution of hydrogen at a Tafel slope of 79 mV dec^{-1} at 290 mV overpotential (10 mA cm^{-2}) is reported. The 140h initial stability test demonstrates that the functionality of polymerized nucleobases can be harnessed for heterogeneous catalysis, i.e., as here demonstrated for the electroconversion of hydrogen.

1. Introduction

To date, the production of hydrogen is fossil-based and relies mainly on steam-reforming of natural gas. In order to transfer hydrogen to a carbon-neutral energy carrier, it has to be electroconvertible using abundant and inexpensive catalyst materials.[1] Instead of commonly used platinum, rhodium and

Dr. H. Coskun, Dr. A. Aljabour, Prof. N. S. Sariciftci, Dr. P. Stadler
Linz Institute for Organic Solar Cells (LIOS)
Institute of Physical Chemistry
Johannes Kepler University Linz
Altenbergerstrasse 69, 4040 Linz, Austria
E-mail: halime.coskun_aljabour@jku.at
Prof. W. Schöfberger
Institute of Organic Chemistry
Johannes Kepler University Linz
4040 Linz, Austria
A. Hinterreiter, Prof. D. Stifter
Center for Surface and Nanoanalytics
Johannes Kepler University Linz
Altenbergerstrasse 69, 4040 Linz, Austria

The ORCID identification number(s) for the author(s) of this article can be found under https://doi.org/10.1002/admi.201901364.

related,[2] functional, bioinspired organics could be optimized for on-par efficient heterogeneous catalysis.[3]

Currently, an enormous effort is put in developing new electrocatalysts, however, many studies still rely on transition metals[4] (mainly phosphides,[5] nitrides, carbides,[6] oxides and sulfides[7] thereof), metal organic frameworks and di-, tri-, and tetrachalcogenides.[8] A rapid movement toward metal-free catalysis is highly coveted and is considered as one of the key aspects in sustainable energy.[9] Hence, to meet the criteria of a good hydrogen electrocatalyst, i.e., having a low binding energy for hydrogen (ΔG_{H*}), providing high exchange current densities (i_0) and low Tafel slopes is a major challenge.[1a,10]

In this work we introduce guanine as one attractive potential molecular electrocatalyst for the hydrogen evolution reaction (HER). We hypothesize that activation of all the conjunct penta-amino functions in the nucleobase can lead to an electrocatalyst that possesses an active site surface density equal to the presently used noble metals.[1a,b,7a,b,10a]

However, the guanine nucleobase is a small molecular system that is electrically insulating and soluble in water.[11] In order to enable its utilization as heterogeneous catalyst, we sought to polymerize guanine and as such create an insoluble, amino-functional and electrically conducting biopolymer.

Guanine shares a structural analogy with aniline, i.e., it possesses one terminal amine and an adverse activated C—H group at the para-positioned imidazole-ring (**Figure 1**). We used this homology and adopted a similar polymerization strategy with the ultimate goal to obtain a functionalized emeraldine-polyguanine (ePG) system. Since the polymerization mechanism for PANI is well-known, we were able to adapt and suggest similar pathways for the polymerization of guanine.[12] Hence, we propose that the primary amine in guanine is initialized under oxidative sulfuric acid surrounding. Next, the generated radical cations couple and finally the propagation reactions take place forming a conductive and doped ePG (Figure 1). Such systems are attractive for hydrogen evolution, since emeraldine is conducting, but compared to polyaniline (PANI), ePG possesses four additional (and potentially catalytic-active) amino-functions. Recently, similarly functionalized conducting

**ADVANCED
SCIENCE NEWS**
www.advancedsciencenews.com

**ADVANCED
MATERIALS
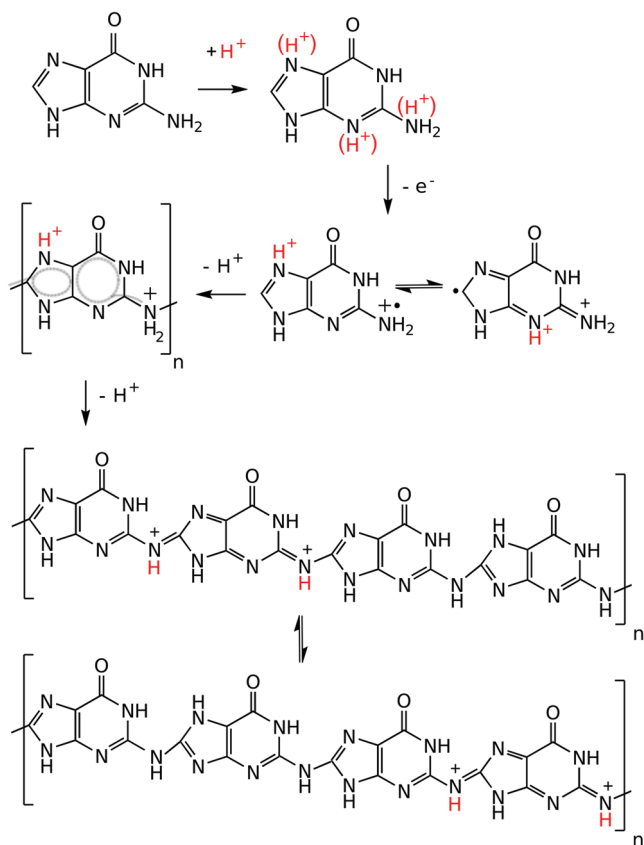INTERFACES**
www.advmatinterfaces.de

Figure 1. Proposed polymerization pathway of protonated conducting biopolymer- emeraldine-polyguanine (ePG). We suggest a reaction mechanism of the oxidative polymerization: initialization by protonation of guanine, the oxidation leading to a mesomeric radical and its subsequent polymerization. The ultimate result is the emeraldine-polyguanine (a conducting analog of the emeraldine salt of polyaniline).

biopolymers such as polydopamine have shown tremendous activity as electrocatalysts.[3a,13]

The polymerization process we applied for guanine bases on an oxidative coupling mechanism. Therefore, the monomer is vaporized and reacted with an oxidant at elevated temperatures (oxidative chemical vapor deposition, oCVD).[13] The oxidative polymerization earlier reported for aniline is adopted here for guanine, however, we modified the process as the nucleobase is a solid and possesses a sublimation point at 360 °C (at ambient pressures). At the same time we had to balance the reactivity of the oxidant in order to suppress the unwanted oxidation of the (nonterminal) amino-sites.[13] We found sulfuric acid as ideal agent, since its moderate oxidation power (e.g., as compared to frequently used agents such as bromine) and its acidity aid the desired terminal amino-carbon coupling and in parallel deactivate the (catalytic) nonterminal amines. As such, we report a quantitative synthetic preparation of protonated conducting ePG by oxidative vapor deposition. The structure determination by Fourier-transform infrared spectroscopy (FTIR), X-ray photoelectron spectroscopy (XPS), and NMR as well as the electrical characterization reveal fingerprint characteristics of ePG which are: i) insolubility in water, ii) increase of the electrical conductivity, iii) infrared-activated vibrations, and iv) the structural conformity of a macromolecule. We deposit ePG

directly on carbon felt and showcase the selective electroreduction of protons to molecular hydrogen in acidic electrolyte solution.

Prior, PANI was investigated in the literature with great interest due to its high electrical conductivity upon doping with acids.[12,14] We demonstrate that proton doping is also possible in (conducting) emeraldine-polyguanine. Based on that we used trifluoromethanesulfonic acid solution (TfOH) as electrolyte to study the electrocatalytic HER. Besides conductivity, TfOH represents a stable and nonreacting (weakly-coordinating) electrolyte system. Here, the proposed HER process can be divided into the adsorption and recombination steps. First, the protons from the acidic solution are adsorbed to the catalytic sites of the ePG electrode. In the following, the atomic hydrogen adatoms recombine to evolve H_2.[15]

The electrocatalytic performance of ePG reaches a Tafel slope of 79 mV dec^{-1} at 290 mV overpotential (at 10 mA cm^{-2}), enhanced by a factor of 4 as compared to polyaniline. We assign the increased activity to the multifunctional sites in guanine leading to the hypothesized aiding character of amino-associated protons as combined dopant and reactant.

In summary, ePG renders a robust and selective hydrogen electrocatalyst. We conclude with further discussing the power of utilizing the strong amino-functionality in the nucleobase (five conjunct-conjugated amino-groups), so that theoretically the catalytic density can ultimately equal the surface kinetics of platinum.[11,12,14,16]

2. Results and Discussions

In this work, we demonstrate the utilization of proton-doping in combination with hydrogen catalysis employing the nucleobase guanine. We present its polymerization using a modified chemical vapor deposition (oCVD) technique, where we apply sulfuric acid as combined oxidation and protonation agent. The united polymerization and protonation was found to direct the synthesis toward a homogeneous conducting polymer (i.e., the polymerization relies on oxidative coupling of the terminal amine and imidazole C−H (Figure 1). Particular the moderate oxidation power of sulfuric acid and in parallel occurring protonation of the amines help to conserve the multiple amino functions by suppressing their unwanted over-oxidation.[3a,12–14] We confirm the formation of ePG salt by structural FTIR, XPS, and solid-state NMR spectroscopy.

The XPS revealed a structural conformity of the ePG formed (**Figure 2**). We first concentrated on the differences between the monomer and the polymer, particularly in the C 1s and N 1s features. The elemental concentrations of the guanine reference (monomer) fit the expected values from literature.[17] Basically, the C 1s peak of the guanine can be fitted with five peaks of equal area (one for each carbon species). Since the carbons C4 and C8 have a very similar binding energy (BE), we combined them in one peak with twice the area (Figure 2a). Similarly, the N 1s spectrum of the monomer reference sample shows two distinct species, which have been attributed to imino- (lower BE) and amino-nitrogen (higher BE) (see Figure S2, Supporting Information).[17] We used the BEs from the monomer as reference for evaluating ePG (Figure 2b). Based on the proposed polymerization reaction we expected a transformation of the C8 carbon into one that has a similar BE as C2. Indeed, the C 1s spectrum of the polymer sample shows a pronounced increase in intensity in the
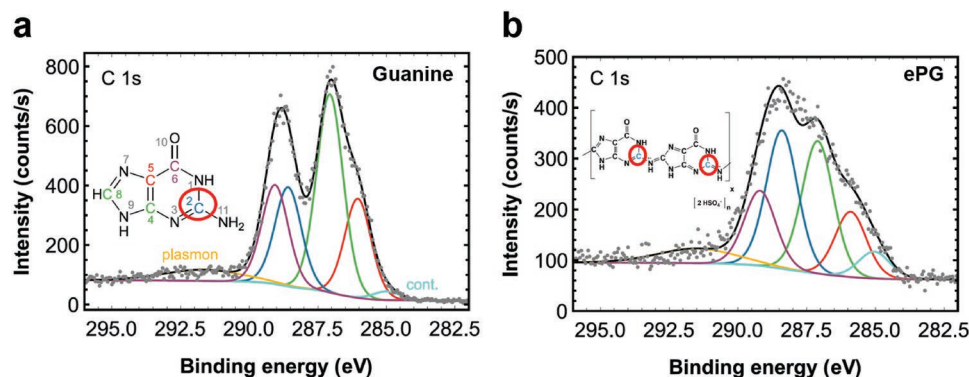
1901364 (2 of 8)

ADVANCED
SCIENCE NEWS
www.advancedsciencenews.com

ADVANCED
MATERIALS
INTERFACES
www.advmatinterfaces.de

Figure 2. X-ray photoelectron spectra of the monomer and polymer a) C 1S spectrum of guanine, b) C 1S spectrum of emeraldine-polyguanine. Especially, changes at positions of C2 and C8 carbons are visible: while the binding energy of C8 is transformed into one that has a similar binding energy as C2, a pronounced increase in intensity in the binding energy of C2 is obtained.

BE region of C2. Also the N 1s spectrum of the polymer exhibits a slightly higher intensity at higher BE as compared to the monomer reference, which explains the decrease of the imino- in favor of amino-functionalities. In addition, we elucidated the BEs of the sulfur 2p peak, as well as the distance between the S 2p and the O 1s peaks that suggest the presence of sulfate as the counter ion in the polymeric structure. However, the elemental ratio of S:O (SO_4) was slightly below the expected 1:4. Again this could be attributed to side reactions involving nitrogen (see Figures S4–S7, Supporting Information).

To confirm these XPS structural findings, we employ complementary high-resolution ^{1}H-, ^{13}C-, and ^{15}N- solid-state NMR spectroscopy to discriminate between the monomeric and the polymeric structure.[18] We show the ^{1}H–[^{13}C,^{15}N] cross-polarization magic angle spinning (CPMAS) spectra of ePG (**Figure 3**b,d) that reveal an increased chemical shift dispersion and an increased line broadening compared to the monomer guanine (Figure 3a,c). This relates to a classic formation of a polymeric structure due to enhanced relaxation times and are in agreement with the earlier results on the XPS.

We also used FTIR spectroscopy to elucidate the structural variety in ePG. In particular, we were interested in the structural changes induced by the new oxidative chemical vapor synthesis. To examine this, we first measured the guanine monomer powder (**Figure 4**).

The FTIR spectrum of the guanine powder is in agreement with the literature values.[19] In contrast, the FTIR spectrum of the ePG is distinctively different: i) it reveals broad polaronic bands between 3536 and 2854 cm^{-1} that partly also overlap with hydrogen-bonding pointing at the formation of a conducting polymers (similar to PANI-emeraldine) and ii) additionally, the presence of free charge careers is indicated by the intense infrared activated vibrations (IRAVs) in the region between 1070 cm^{-1} and 840 cm^{-1}. IRAV bands represent a fingerprint feature of the electron-phonon coupling in all conducting polymers (as results of oscillator enhancement in the MIR).[20] The sharp peaks between 1643 to 1257 cm^{-1}, attributed to the stretching vibrations of imine, amine and carbonyl features, respectively.

The as-formed macromolecule possesses an intrinsic electrical conductivity of 10^{-6} S cm^{-1} at 300K (**Figure 5**). We measured this value in ePG films using the van der Pauw geometry in dry helium atmosphere. At ambient conditions,

and particularly after treatment with acids (e.g., sulfuric acid and TfOH), the conductivity rises. Thus, analogous to PANI, the conductivity depends strongly on the acidity of the environment. While in vacuo the nonprotonated emeraldine-base is highly insulating, exposure to different acids increases the conductivity by several orders of magnitude reaching ultimately 1 × 10^{-4} S cm^{-1} in TfOH. We show that there exists a relation between acid strength (hence protonation quantity, pKa) and the electrical conductivity (Figure 5). The electrical conductivity of ePG, however, is in general below PANI, but this may not affect directly its electrocatalytic HER activity, which we find superior due to functional improvement in its structure.

The HER activity of ePG coated carbon felt (CF) electrodes we tested at room temperature in an H-cell configuration, and plotted the polarization scans all referred to RHE potential values (**Figure 6**a). The reference electrode Ag/AgCl (3 M KCl) is calibrated using reversible hydrogen electrode, accordingly (see Figure S9, Supporting Information) and the onset potential of +197 mV versus SHE is taken into account for the conversion into RHE potential values (Equation (1))

$$E_{(RHE)} = E^0 + E_{(Ag/AgCl)} + 0.059\,pH \tag{1}$$

In Figure 6b, the HER overpotentials for Pt, ePG, and PANI are shown as a function of the logarithm of the current density to derive the Tafel slope. Qualitatively, it is seen that the Tafel slope of PANI (166 mV dec^{-1}) is significantly above that of ePG (and Pt). The kinetic activity of ePG (79 mV dec^{-1}) is substantially enhanced. We attribute the superior performance of ePG to the fact that the different predominant amine groups in the biopolymer chain get protonated and thus exhibit a greater electron affinity toward the hydrogen evolution reactions, while PANI only contains one (terminal) amine leading to lower functional density. Note that the electrocatalytic performance of emeraldine-polyguanine is promising, however, yet under-developed as compared to the state-of-the-art metal HER catalysts.[1a,b,7a,b,10a] The novelty of this study is associated to the introduction of a new, organic, metal-free, emeraldine analogous electrocatalyst, first time synthesized through oxidative chemical vapor deposition. We show that proton-doped polyguanine improves the electrochemical hydrogen evolution in acidic media, where the optimum balance in terms of
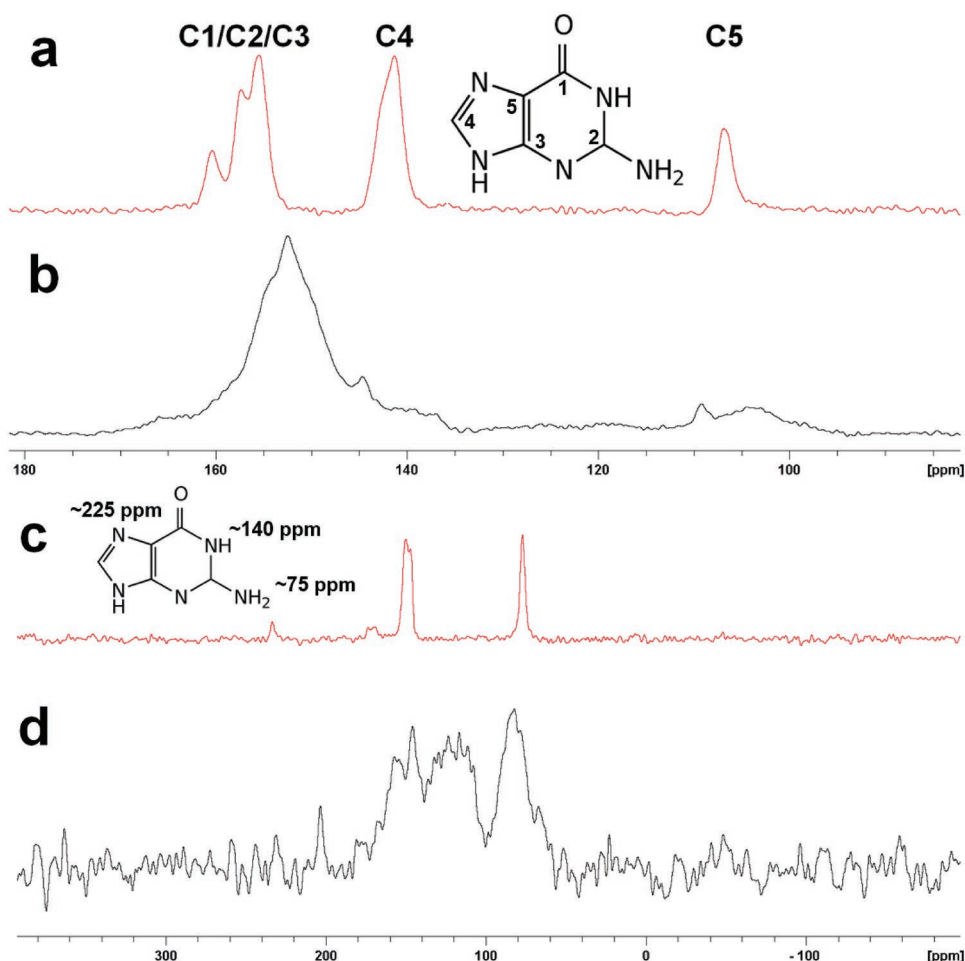
Figure 3. Solid state ^{1}H-^{13}C-CPMAS and ^{1}H-^{15}N-CPMAS NMR spectra of a,c) guanine and b,d) emeraldine-polyguanine (ePG). The polymer shows an increased chemical shift dispersion and increased line broadening as compared to the monomer that underlines the proposed formation of a polymeric structure due to enhanced relaxation times.
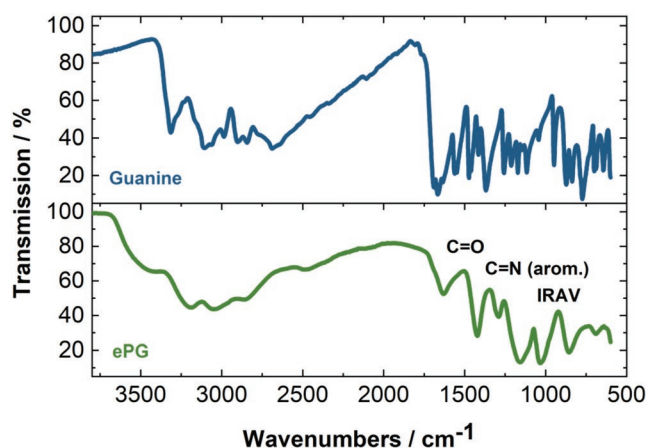

Figure 4. FTIR spectrum of guanine monomer as powder (blue) and emeraldine-polyguanine (ePG, green). The formation of the conducting polymer is verified by broad polaronic absorption in the region between 3536 and 2854 cm^{-1} and the emergence of the infrared activated vibrations at 1070 cm^{-1} and below.
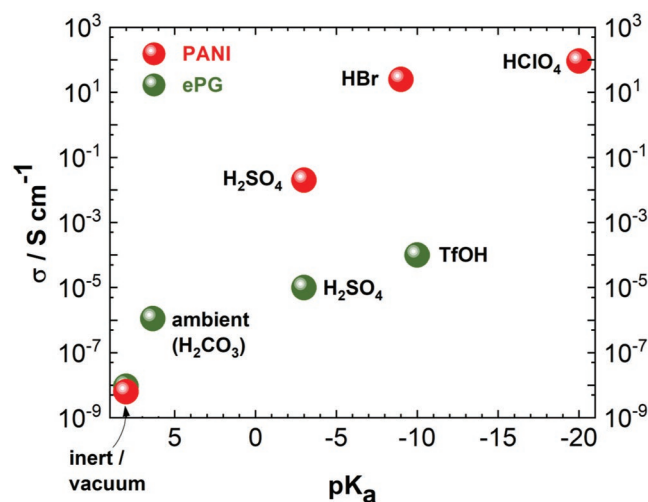
Figure 5. Conductivities of emeraldine-polyguanine (green) measured at different acidic environment in comparison to PANI (red) in different doped and undoped states. The analogy between these polymeric systems is expressed by the increase of conductivity upon proton-enriched surrounding, indicated by the pK_a of the acid.
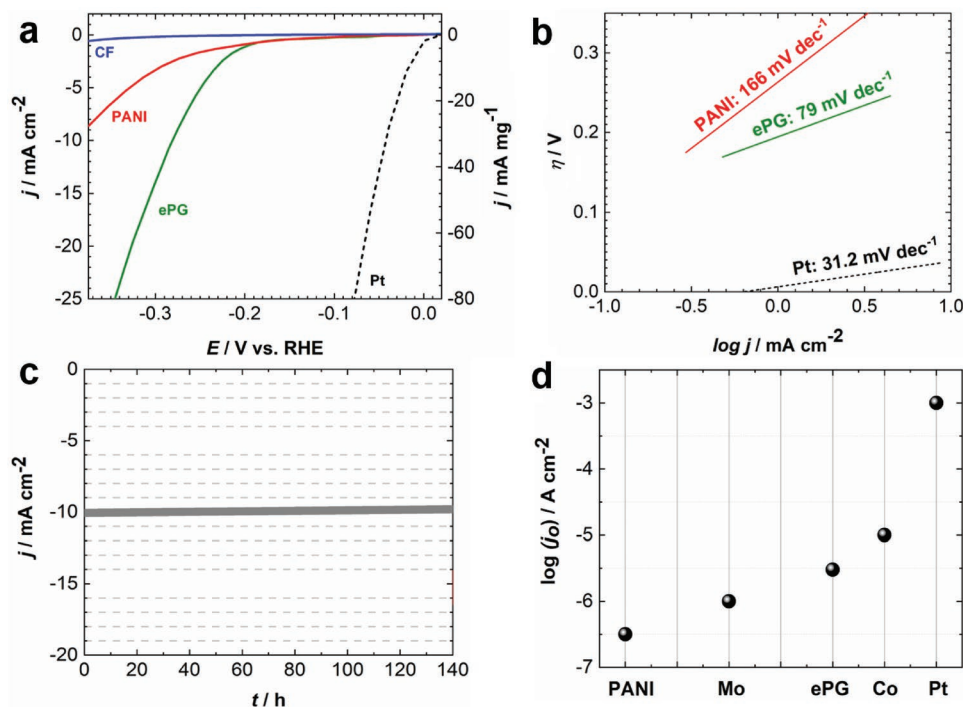
1901364 (4 of 8)

Figure 6. Electrochemical characterization including a) polarization scans recorded at 10 mV s^{-1}, b) Tafel plots, in which the overpotential is plotted as a function of log (j) for Pt, ePG, and PANI systems, c) constant potential electrolysis at −290 mV versus RHE using graphite rod as counter electrode for 140 h of operation, d) comparison of emeraldine-polyguanine: the logarithm of exchange current density with catalytic metals and polyaniline reveals a position between molybdenum and cobalt for ePG.[23]

electrical conductivity, catalytic activity and reduction stability is found. The electrocatalytic performance is comparable to molybdenum[1a,b,7a,b,10a,21] revealing a Tafel slope as low as 79 mV dec^{-1} and an overpotential of 290 mV at 10 mA cm^{-2} Faradaic current demonstrated in a 140 h continuous hydrogen electrolysis (see Table S1, Supporting Information).

We find the Tafel slope for platinum foil surface is in agreement with those reported in literature.[4c,6c,7c,d,21,22] Further, the Tafel slope is used in order to extract the exchange current density J_o for ePG. Hereby, the J_o value is compensated by the actual electrochemical active area, determined through electrochemical impedance measurements (see Table S2, Supporting Information) as 18.73 cm^2 (see the Supporting Information). The exchange current density J_o for ePG results in 3×10^{-6} A cm^{-2} (see Figure S10, Supporting Information). This value positions emeraldine-polyguanine between molybdenum and cobalt in exchange current density (Figure 6d).[1a,b,5b,7a,b,10a,21]

Interestingly, the electrochemical stability is especially crucial for the organic and biological systems in extreme and harsh acidic conditions. To test the long-term stability of the PG samples studied in this work, we conducted constant potential electrolysis at −290 mV versus RHE for 140 h. Based on

the representative chronoamperometric scans (Figure 6c), we find extensive durability for ePG HER electrocatalyst, even after 140 h of continuous operation.

We finally crosschecked emeraldine-polyguanine deposited on carbon felt electrodes by the scanning electron microscopy. As shown in **Figure 7**a, before constant potential electrolysis
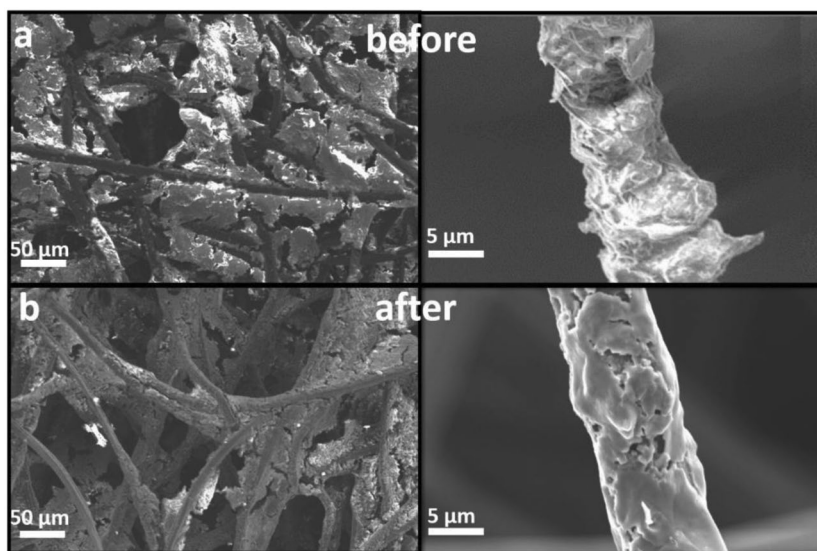

Figure 7. SEM images of emeraldine-polyguanine deposited on carbon felt, a) before and b) after constant potential electrolysis at −290 mV versus RHE.

the fiber networks are widely covered by ePG, so that the electrocatalyst infiltrated into the sponge-type supporting electrode. After the long-term stability experiment it can be seen that the ePG catalyst still remains on the CF fibers (Figure 7b) with some less dense regions on the CF electrode.

3. Conclusion

In this study, we show the utilization of an alternative biopolymer, derived from guanine, one of the building blocks of the DNA macromolecule, as hydrogen cathode for HER electrocatalysis. We have synthesized ePG from the vapor phase using the oCVD and achieved the polymerization and the oxidative doping of the resulting polymer in a facile single step reaction from the vapor phase of the guanine monomer with sulfuric acid. As compared to PANI, one of the well-known conducting polymers, we find analogies in structure and conductivity increase by proton doping. Our results suggest the fact that the prevalent amines in ePG get protonated and thus have superior electron affinity to accelerate the hydrogen evolution steps in $(H^+ + e^- \rightarrow H_{ADS})$ and $(H_{ADS} + H_{ADS} \rightarrow H_2)$ reactions.

Indeed, paired with HER electrocatalyst performance (Tafel slope of 79 mV dec^{-1} at an overpotential of 290 mV at 10 mA cm^{-2}) and a stable operation of 140 h in a strong 1 M TfOH, emeraldine-polyguanine demonstrates promising abilities as an alternative biopolymer electrocatalyst for the future.

4. Experimental Section

Synthesis: oCVD was used for the deposition of ePG directly on CF (10 mm × 10 mm, SGL Group, The Carbon Company) (**Figure 8**). These electrodes were applied in electrochemical studies. For conductivity measurements sapphire substrates (10 mm × 10 mm × 0.5 mm, CrysTec Kristalltechnologie) were utilized with Cr/Au (8 nm/80 nm) electrodes in the van der Pauw geometry. All substrates were treated with acetone, isopropanol, Hellmanex-detergent (Hellma, 70 °C), and deionized water prior usage. Chromium/gold electrodes were deposited by physical vapor deposition through a shadow mask. For the ePG-synthesis, guanine (Sigma-Aldrich) was dried 15 min at 100 °C. For the polymerization oxidative chemical vapor deposition technique was used. The equipment
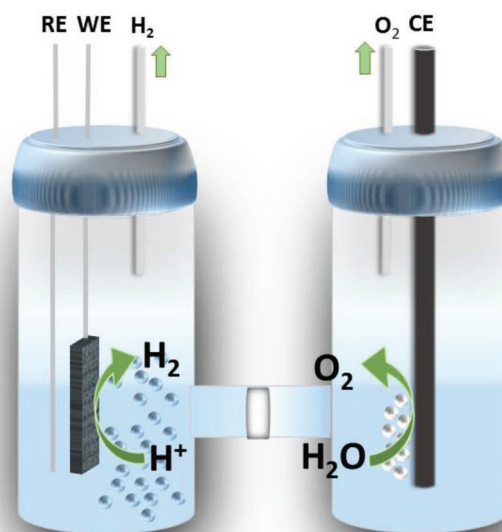
Figure 9. Experimental setup for electrochemical characterization. A standard three-electrode arrangement is used in an H-Cell configuration, with PG as WE, Ag/AgCl as RE, and graphite rod as CE all in a 1 M trifluoromethanesulfonic acid.

consisted of a tube furnace (Nabertherm company; glass tube length: 110 cm; tube diameter: 5 cm). In zone 2, the temperature was set constant to 360 °C in order to evaporate guanine. Nitrogen (3 L min^{-1}) was used as carrier gas in a laminar flow. The entire process was carried out at atmospheric pressure (1 atm). In zone 1, sulfuric acid (95–97%, J.T. Baker) and sodium sulfate (≥99.0%, Sigma-Aldrich) were prepared. Upon heating up to 240 °C, the acid was vaporized and immediately reacted with the gas-phase guanine. The desired substrates were placed in between zones 2 and 1 so that the emeraldine-polyguanine deposition could take place.

Electrochemical Characterization: For the electrochemical characterization the electrodes were immediately installed as working electrode. The as-prepared ePG, PANI, and blank carbon felt electrodes were electrochemically characterized for hydrogen evolution using an H-Cell configuration (see **Figure 9**). Electrochemical experiments were conducted using a JAISSLE Potentiostat Galvanostat IMP 88 PC. Carbon-felt electrodes (and the catalyst coated electrodes) were set as working electrodes, Ag/AgCl (3 M KCl, +197 mV vs SHE) was set as reference electrode and graphite rod (Alfa Aesar, 99.9995%) as counter electrode.

Long-term chronoamperometry experiments were conducted by using graphite rod as counter electrode to prevent potential contamination with platinum on the working electrode. 1 M TfOH (98%, Sigma-Aldrich) was used as electrolyte solution (pH ≈ 0). Distance was maintained deliberately from sulfuric acid, considered as the standard HER solution, to achieve superior stability and avoid possible side reactions. Hereby, a quantitative Faradaic yield of almost 100% hydrogen was attained, as detected by gas chromatography. For comparison, the CV and chronoamperometry scans in 0.5 M H$_2$SO$_4$ are provided in the Supporting Information (see Figures S12 and S13, Supporting Information).

The anodic and the cathodic compartments of the H-cell were separated by a diaphragm. Before chronoamperometry, the sealed compartments of the cell were purged with N$_2$ gas for 1 h. All results are given relative to the RHE.
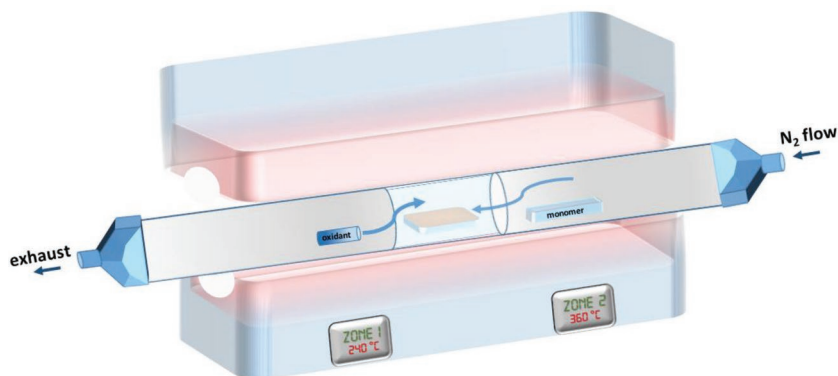

Figure 8. Nabertherm Tube Furnace for oxidative chemical vapor deposition of guanine. The guanine monomer is placed at zone 2, the sulfuric acid at zone 1, and the substrate in between zones 1 and 2.

Cyclic voltamogram scans (10 mV s^{-1}) and chronoamperometric scans were conducted under stirring conditions of the electrolyte solution in the cathode space by 300 rpm. A sealed compartment was used to frequently control the quantitative H$_2$ yield, using a TRACE Ultra Gas Chromatograph equipped with a thermal conductivity detector (TCD). No other side-product was found in this system.[3a,24]

Supporting Information

Supporting Information is available from the Wiley Online Library or from the author.

Conflict of Interest

The authors declare no conflict of interest.

[1] a) J. D. Benck, Z. Chen, L. Y. Kuritzky, A. J. Forman, T. F. Jaramillo, *ACS Catal.* **2012**, *2*, 1916; b) J. Bonde, P. G. Moses, T. F. Jaramillo, J. K. Nørskov, I. Chorkendorff, *Faraday Discuss.* **2009**, *140*, 219; c) R. Bose, V. R. Jothi, B. Koh, C. Jung, S. C. Yi, *Small* **2018**, *14*, 1703862; d) V. Y. Fominski, R. I. Romanov, D. V. Fominski, P. S. Dzhumaev, I. A. Troyan, *Opt. Laser Technol.* **2018**, *102*, 74; e) J. Hu, B. Huang, C. Zhang, Z. Wang, Y. An, D. Zhou, H. Lin, M. K. H. Leung, S. Yang, *Energy Environ. Sci.* **2017**, *10*, 593; f) J. Hu, C. X. Zhang, X. Y. Meng, H. Lin, C. Hu, X. Long, S. H. Yang, *J. Mater. Chem. A* **2017**, *5*, 5995.

[2] H. Zhang, P. An, W. Zhou, B. Y. Guan, P. Zhang, J. Dong, X. W. Lou, *Sci. Adv.* **2018**, *4*, eaao6657.

[3] a) H. Coskun, A. Aljabour, P. De Luna, D. Farka, T. Greunz, D. Stifter, M. Kus, X. L. Zheng, M. Liu, A. W. Hassel, W. Schofberger, E. H. Sargent, N. S. Sariciftci, P. Stadler, *Sci. Adv.* **2017**, *3*, e1700686; b) Z. W. Seh, J. Kibsgaard, C. F. Dickens, I. Chorkendorff, J. K. Nørskov, T. F. Jaramillo, *Science* **2017**, 355.

[4] a) J. Li, P. Liu, Y. Qu, T. Liao, B. Xiang, *Int. J. Hydrogen Energy* **2018**, *43*, 2601; b) Y. B. Mollamahale, N. Jafari, D. Hosseini, *Mater. Lett.* **2018**, *213*, 15; c) C. Tan, Z. Luo, A. Chaturvedi, Y. Cai, Y. Du,

Y. Gong, Y. Huang, Z. Lai, X. Zhang, L. Zheng, X. Qi, M. H. Goh, J. Wang, S. Han, X.-J. Wu, L. Gu, C. Kloc, H. Zhang, *Adv. Mater.* **2018**, *30*, 1705509.

[5] a) J. Kibsgaard, T. F. Jaramillo, *Angew. Chem., Int. Ed.* **2014**, *53*, 14433; b) E. J. Popczun, C. G. Read, C. W. Roske, N. S. Lewis, R. E. Schaak, *Angew. Chem., Int. Ed.* **2014**, *53*, 5427; c) P. Xiao, M. A. Sk, L. Thia, X. M. Ge, R. J. Lim, J. Y. Wang, K. H. Lim, X. Wang, *Energy Environ. Sci.* **2014**, *7*, 2624.

[6] a) S. Y. Jing, L. S. Zhang, L. Luo, J. J. Lu, S. B. Yin, P. K. Shen, P. Tsiakaras, *Appl. Catal., B* **2018**, *224*, 533; b) F. Li, X. Zhao, J. Mahmood, M. S. Okyay, S.-M. Jung, I. Ahmad, S.-J. Kim, G.-F. Han, N. Park, J.-B. Baek, *ACS Nano* **2017**, *11*, 7527; c) M. Miao, J. Pan, T. He, Y. Yan, B. Y. Xia, X. Wang, *Chem. - Eur. J.* **2017**, *23*, 10947.

[7] a) A. B. Laursen, S. Kegnæs, S. Dahl, I. Chorkendorff, *Energy Environ. Sci.* **2012**, *5*, 5577; b) H. Li, C. Tsai, A. L. Koh, L. Cai, A. W. Contryman, A. H. Fragapane, J. Zhao, H. S. Han, H. C. Manoharan, F. Abild-Pedersen, J. K. Nørskov, X. Zheng, *Nat. Mater.* **2016**, *15*, 48; c) D. Voiry, M. Salehi, R. Silva, T. Fujita, M. Chen, T. Asefa, V. B. Shenoy, G. Eda, M. Chhowalla, *Nano Lett.* **2013**, *13*, 6222; d) D. Voiry, H. Yamaguchi, J. Li, R. Silva, D. C. B. Alves, T. Fujita, M. Chen, T. Asefa, V. B. Shenoy, G. Eda, M. Chhowalla, *Nat. Mater.* **2013**, *12*, 850; e) J. Xie, H. Zhang, S. Li, R. Wang, X. Sun, M. Zhou, J. Zhou, X. W. Lou, Y. Xie, *Adv. Mater.* **2013**, *25*, 5807.

[8] a) M. I. Abdullah, A. Hameed, N. Zhang, M. Ma, *Adv. Mater. Interfaces* **2019**, *6*, 1900586; b) X. Dong, H. Yan, Y. Jiao, D. Guo, A. Wu, G. Yang, X. Shi, C. Tian, H. Fu, *J. Mater. Chem. A* **2019**, *7*, 15823; c) H. Jin, X. Liu, S. Chen, A. Vasileff, L. Li, Y. Jiao, L. Song, Y. Zheng, S.-Z. Qiao, *ACS Energy Lett.* **2019**, *4*, 805; d) T. Ling, T. Zhang, B. Ge, L. Han, L. Zheng, F. Lin, Z. Xu, W. B. Hu, X. W. Du, K. Davey, *Adv. Mater.* **2019**, *31*, 1807771; e) X. Liu, Y. Jiao, Y. Zheng, K. Davey, S.-Z. Qiao, *J. Mater. Chem. A* **2019**, *7*, 3648; f) J. McAllister, N. A. Bandeira, J. C. McGlynn, A. Y. Ganin, Y.-F. Song, C. Bo, H. N. Miras, *Nat. Commun.* **2019**, *10*, 370; g) Z. Pu, J. Zhao, I. S. Amiinu, W. Li, M. Wang, D. He, S. Mu, *Energy Environ. Sci.* **2019**, *12*, 952; h) S. A. Shah, X. Shen, M. Xie, G. Zhu, Z. Ji, H. Zhou, K. Xu, X. Yue, A. Yuan, J. Zhu, *Small* **2019**, *15*, 1804545; i) M. Sheng, B. Jiang, B. Wu, F. Liao, X. Fan, H. Lin, Y. Li, Y. Lifshitz, S.-T. Lee, M. Shao, *ACS Nano* **2019**, *13*, 2786; j) S. Ye, F. Luo, Q. Zhang, P. Zhang, T. Xu, Q. Wang, D. He, L. Guo, Y. Zhang, C. He, *Energy Environ. Sci.* **2019**, *12*, 1000; k) J. Zhu, Z.-C. Wang, H. Dai, Q. Wang, R. Yang, H. Yu, M. Liao, J. Zhang, W. Chen, Z. Wei, *Nat. Commun.* **2019**, *10*, 1348.

[9] a) M. D. Hossain, Z. Liu, M. Zhuang, X. Yan, G. L. Xu, C. A. Gadre, A. Tyagi, I. H. Abidi, C. J. Sun, H. Wong, *Adv. Energy Mater.* **2019**, *9*, 1803689; b) X. F. Lu, L. Yu, J. Zhang, X. W. Lou, *Adv. Mater.* **2019**, 1900699; c) C. N. R. Rao, M. Chhetri, *Adv. Mater.* **2019**, *31*, 1803668; d) M. H. Suliman, A. Adam, M. N. Siddiqui, Z. H. Yamani, M. Qamar, *Carbon* **2019**, *144*, 764.

[10] a) T. F. Jaramillo, K. P. Jørgensen, J. Bonde, J. H. Nielsen, S. Horch, I. Chorkendorff, *Science* **2007**, *317*, 100; b) Q. Lu, J. Rosen, Y. Zhou, G. S. Hutchings, Y. C. Kimmel, J. G. Chen, F. Jiao, *Nat. Commun.* **2014**, *5*, 3242; c) D. Voiry, H. S. Shin, K. P. Loh, M. Chhowalla, *Nat. Rev. Chem.* **2018**, *2*, 105; d) Z. Zhuang, Y. Li, Z. Li, F. Lv, Z. Lang, K. Zhao, L. Zhou, L. Moskaleva, S. Guo, L. Mai, *Angew. Chem., Int. Ed.* **2018**, *57*, 496.

[11] M. Arvand, M. Sanayeei, S. Hemmati, *Biosens. Bioelectron.* **2018**, *102*, 70.

[12] J.-C. Chiang, A. G. MacDiarmid, *Synth. Met.* **1986**, *13*, 193.

[13] H. Coskun, A. Aljabour, L. Uiberlacker, M. Strobel, S. Hild, C. Cobet, D. Farka, P. Stadler, N. S. Sariciftci, *Thin Solid Films* **2018**, *645*, 320.

[14] a) W.-S. Huang, B. D. Humphrey, A. G. MacDiarmid, *J. Chem. Soc., Faraday Trans. 1* **1986**, *82*, 2385; b) A. G. MacDiarmid, A. J. Epstein, *Faraday Discuss. Chem. Soc.* **1989**, *88*, 317.

[15] a) G. Chen, T. Wang, J. Zhang, P. Liu, H. Sun, X. Zhuang, M. Chen, X. Feng, *Adv. Mater.* **2018**, *30*, 1706279; b) J. Zhang, J. Wu, H. Guo, W. Chen, J. Yuan, U. Martinez, G. Gupta, A. Mohite, P. M. Ajayan, J. Lou, *Adv. Mater.* **2017**, *29*, 1701955; c) Q. Zhang, W. Wang, J. Zhang, X. Zhu, Q. Zhang, Y. Zhang, Z. Ren, S. Song, J. Wang, Z. Ying, R. Wang, X. Qiu, T. Peng, L. Fu, *Adv. Mater.* **2018**, *30*, 1707123.

[16] a) S. Das, R. Ghosh, P. Routh, A. Shit, S. Mondal, A. Panja, A. K. Nandi, *ACS Appl. Nano Mater.* **2018**, *1*, 2306; b) J. X. Feng, S. Y. Tong, Y. X. Tong, G. R. Li, *J. Am. Chem. Soc.* **2018**, *140*, 5118; c) J. W. Ma, M. Wang, G. Y. Lei, G. L. Zhang, F. B. Zhang, W. C. Peng, X. B. Fan, Y. Li, *Small* **2018**, *14*, 1702895; d) M. H. Naveen, N. G. Gurudatt, Y. B. Shim, *Appl. Mater. Today* **2017**, *9*, 419; e) K. E. Ramohlola, G. R. Monana, M. J. Hato, K. D. Modibane, K. M. Molapo, M. Masikini, S. B. Mduli, E. I. Iwuoha, *Composites, Part B* **2018**, *137*, 129; f) E. Cam, N. A. Tanik, I. Cerkez, E. Demirkan, Y. Aykut, *J. Appl. Polym. Sci.* **2018**, *135*, 45567; g) L. D'Agostino, *Nanoscale* **2018**, *10*, 12268; h) S. H. Gao, H. J. Li, M. J. Li, C. P. Li, L. R. Qian, B. H. Yang, *J. Solid State Electrochem.* **2018**, *22*, 3245; i) K. Hinrichs, S. D. Silaghi, C. Cobet, N. Esser, D. R. T. Zahn, *Phys. Status Solidi B* **2005**, *242*, 2681; j) S. Jesny, K. Girish Kumar, *J. Electroanal. Chem.* **2017**, *801*, 153; k) Ks. Siddegowda, B. Mahesh, N. Kumara Swamy, *Sens. Actuators, A* **2018**, *280*, 277; l) W. Li, J. Jin, X. Q. Liu, L. Wang, *Langmuir* **2018**, *34*, 8092; m) N. J. Popczun, L. Breuer, A. Wucher, N. Winograd, *J. Phys. Chem. C* **2017**, *121*, 8931; n) A. S. Rad, S. M. Aghaei, *Curr. Appl. Phys.* **2018**, *18*, 133; o) W. Shi, J. Yu, H. E. Katz, *Sens. Actuators, B* **2018**, *254*, 940; p) W. Shi, Y. F. Zheng, A. D. Taylor, J. S. Yu, H. E. Katz, *Appl. Phys. Lett.* **2017**, *111*, 043301; q) M. L. Wang, M. Z. Cui, W. F. Liu, X. G. Liu, B. S. Xu, *Electroanalysis* **2018**, *30*, 842; r) T. Yamada, K. Shirasaka, A. Takano,

M. Kawai, *Surf. Sci.* **2004**, *561*, 233; s) L. Zhang, J. Zhang, *Biosens. Bioelectron.* **2018**, *110*, 218.

[17] a) V. Feyer, O. Plekan, F. Šutara, V. Cháb, V. Matolín, K. C. Prince, *Surf. Sci.* **2011**, *605*, 361; b) M. Furukawa, T. Yamada, S. Katano, M. Kawai, H. Ogasawara, A. Nilsson, *Surf. Sci.* **2007**, *601*, 5433.

[18] a) M. Dračínský, M. Šála, B. Klepetářová, J. Šebera, J. Fukal, V. Holečková, Y. Tanaka, R. Nencka, V. Sychrovský, *J. Phys. Chem. B* **2016**, *120*, 915; b) R. Pohl, O. Socha, P. Slavíček, M. Šála, P. Hodgkinson, M. Dračínský, *Faraday Discuss.* **2018**, *212*, 331.

[19] a) K. P. Gan, M. Yoshio, Y. Sugihara, T. Kato, *Chem. Sci.* **2018**, *9*, 576; b) D. Gur, M. Pierantoni, N. Elool Dov, A. Hirsh, Y. Feldman, S. Weiner, L. Addadi, *Cryst. Growth Des.* **2016**, *16*, 4975.

[20] a) C. Cobet, J. Gasiorowski, R. Menon, K. Hingerl, S. Schlager, M. S. White, H. Neugebauer, N. S. Sariciftci, P. Stadler, *Sci. Rep.* **2016**, *6*, 35096; b) C. Enengl, S. Enengl, M. Havlicek, P. Stadler, E. D. Glowacki, M. C. Scharber, M. White, K. Hingerl, E. Ehrenfreund, H. Neugebauer, *Adv. Funct. Mater.* **2015**, *25*, 6679; c) A. Fisher, W. Hayes, D. Wallace, *J. Phys.: Condens. Matter* **1989**, *1*, 5567; d) A. Ugur, F. Katmis, M. Li, L. Wu, Y. Zhu, K. K. Varanasi, K. K. Gleason, *Adv. Mater.* **2015**, *27*, 4604.

[21] P. Xiao, M. A. Sk, L. Thia, X. Ge, R. J. Lim, J.-Y. Wang, K. H. Lim, X. Wang, *Energy Environ. Sci.* **2014**, *7*, 2624.

[22] R. He, J. Hua, A. Zhang, C. Wang, J. Peng, W. Chen, J. Zeng, *Nano Lett.* **2017**, *17*, 4311.

[23] S. Trasatti, *J. Electroanal. Chem. Interfacial Electrochem.* **1972**, *39*, 163.

[24] a) A. Aljabour, D. H. Apaydin, H. Coskun, F. Ozel, M. Ersoz, P. Stadler, N. S. Sariciftci, M. Kus, *ACS Appl. Mater. Interfaces* **2016**, *8*, 31695; b) A. Aljabour, H. Coskun, D. H. Apaydin, F. Ozel, A. W. Hassel, P. Stadler, N. S. Sariciftci, M. Kus, *Appl. Catal., B* **2018**, *229*, 163.